Gating modifier toxins isolated from spider venom: Modulation of voltage-gated sodium channels and the role of lipid membranes

Received for publication, February 25, 2018, and in revised form, April 25, 2018 Published, Papers in Press, April 27, 2018, DOI 10.1074/jbc.RA118.002553

Akello J. Agwa[‡], Steve Peigneur[§], Chun Yuen Chow[‡], Nicole Lawrence[‡], David J. Craik[‡], Jan Tytgat[§], Glenn F. King[‡], Sónia Troeira Henriques[‡], and Christina I. Schroeder[‡1]

From the [‡]Institute for Molecular Bioscience, University of Queensland, Brisbane, Queensland 4072, Australia and [§]Laboratory of Toxicology and Pharmacology, University of Leuven (KU Leuven), 3000 Leuven, Belgium

Edited by Mike Shipston

Gating modifier toxins (GMTs) are venom-derived peptides isolated from spiders and other venomous creatures and modulate activity of disease-relevant voltage-gated ion channels and are therefore being pursued as therapeutic leads. The amphipathic surface profile of GMTs has prompted the proposal that some GMTs simultaneously bind to the cell membrane and voltage-gated ion channels in a trimolecular complex. Here, we examined whether there is a relationship among spider GMT amphipathicity, membrane binding, and potency or selectivity for voltage-gated sodium (Na_V) channels. We used NMR spectroscopy and *in silico* calculations to examine the structures and physicochemical properties of a panel of nine GMTs and deployed surface plasmon resonance to measure GMT affinity for lipids putatively found in proximity to Na_V channels. Electrophysiology was used to quantify GMT activity on $Na_V1.7$, an ion channel linked to chronic pain. Selectivity of the peptides was further examined against a panel of Na_V channel subtypes. We show that GMTs adsorb to the outer leaflet of anionic lipid bilayers through electrostatic interactions. We did not observe a direct correlation between GMT amphipathicity and affinity for lipid bilayers. Furthermore, GMT–lipid bilayer interactions did not correlate with potency or selectivity for Na_Vs. We therefore propose that increased membrane binding is unlikely to improve subtype selectivity and that the conserved amphipathic GMT surface profile is an adaptation that facilitates simultaneous modulation of multiple Na_Vs.

This work was supported by Australian National Health and Medical Research Council Project Grant APP1080405 (to C. I. S. and S. T. H.) and Program Grant APP1072113 and Principal Research Fellowship APP1044414 (to G. F. K.); Australian Research Council (ARC) Future Fellowships FT160100055 (to C. I. S.) and FT150100398 (to S. T. H.) and Australian Laureate fellowship FL150100146 (to D. J. C.); Central Europe Leuven Strategic Alliance Grant CELSA/17/047–BOF/ISP (to J. T.); and University of Queensland International Postgraduate Scholarships (to A. J. A. and C. Y. C.). The authors declare that they have no conflicts of interest with the contents of this article.

This article contains Tables S1–S3 and Figs. S1 and S2.

The atomic coordinates and structure factors (codes 6BR0 and 6BTV) have been deposited in the Protein Data Bank (http://wwpdb.org/).

The NMR data in this paper have been submitted to the Biological Magnetic Resonance Data Bank under accession nos. 30376 (CcoTx-I) and 30377 (CcoTx-II).

[1] To whom correspondence should be addressed: Institute for Molecular Bioscience, University of Queensland, Brisbane, Queensland 4072, Australia. Tel.: 61-3346-2021; E-mail: c.schroeder@imb.uq.edu.au.

Gating modifier toxins (GMTs)[2] extracted from spider venom are a class of peptides that are valuable probes for studying the physiology and pharmacology of voltage-gated ion channels (1–4). GMTs alter the gating kinetics of voltage-gated ion channels (4), which are transmembrane proteins integral to a range of physiological processes in humans (1, 5, 6). These GMTs contain six Cys residues arranged to form an inhibitory cystine knot motif (7). In addition, these peptides share a conserved amphipathic surface profile characterized by a high proportion of hydrophobic amino acid residues, such as Trp, Tyr, and Phe, surrounded by a ring of cationic residues, including Arg and Lys, that typically promote peptide–membrane interactions (Fig. 1, *A* and *B*) (8).

Several GMTs, including GsMTx-IV, HaTx-I, VsTx-I, ProTx-I, ProTx-II, and SgTx-I, have been shown to bind to model membranes (8–12). The concept of a trimolecular lipid-peptide-channel complex has subsequently been proposed to exist in interactions between GMTs, voltage-gated ion channels, and the lipid membrane (10, 13, 14). A trimolecular complex presents the possibility for a novel approach to rational drug design whereby the cell membrane is considered as a third component in addition to the traditional approach, which only takes into account the transmembrane protein and the modulatory ligand (10, 14, 15).

The objective of the current study was to determine whether there is an overall relationship between the amphipathic surface profile of GMTs and their ability to bind lipid membranes and modulate voltage-gated ion channels. Electrophysiology was used to examine potency of the peptides at voltage-gated sodium channel 1.7 ($Na_V1.7$), a transmembrane protein that is currently being pursued as a target for development of therapeutics for chronic pain (5, 16). GMTs are likely to show toxicity in mammals if they show activity at off-target Na_Vs; therefore, $Na_V1.2$, $Na_V1.4$, $Na_V1.5$, and $Na_V1.6$ were included to study whether there is a relationship between GMT amphipathicity, affinity for lipid bilayers, and off-target selec-

[2] The abbreviations used are: GMT, gating modifier toxin; CHOL, cholesterol; C1P, ceramide 1-phosphate; ACN, acetonitrile; HEK, human embryonic kidney; LUV, large unilamellar vesicle; P/L, peptide/lipid; PI, L-α-phosphatidylinositol; POPC, 1-palmitoyl-2-oleoyl-*sn*-glycero-3-phosphocholine; POPS, 1-palmitoyl-2-oleoyl-*sn*-glycero-3-phospho-L-serine; SM, sphingomyelin; Smase D, sphingomyelinase D; SPR, surface plasmon resonance; SUV, small unilamellar vesicle; Na_v, voltage-gated sodium; RP-HPLC, reverse-phase HPLC; SASA, solvent-accessible surface area; PG, phosphatidylglycerol; PDB, Protein Data Bank.

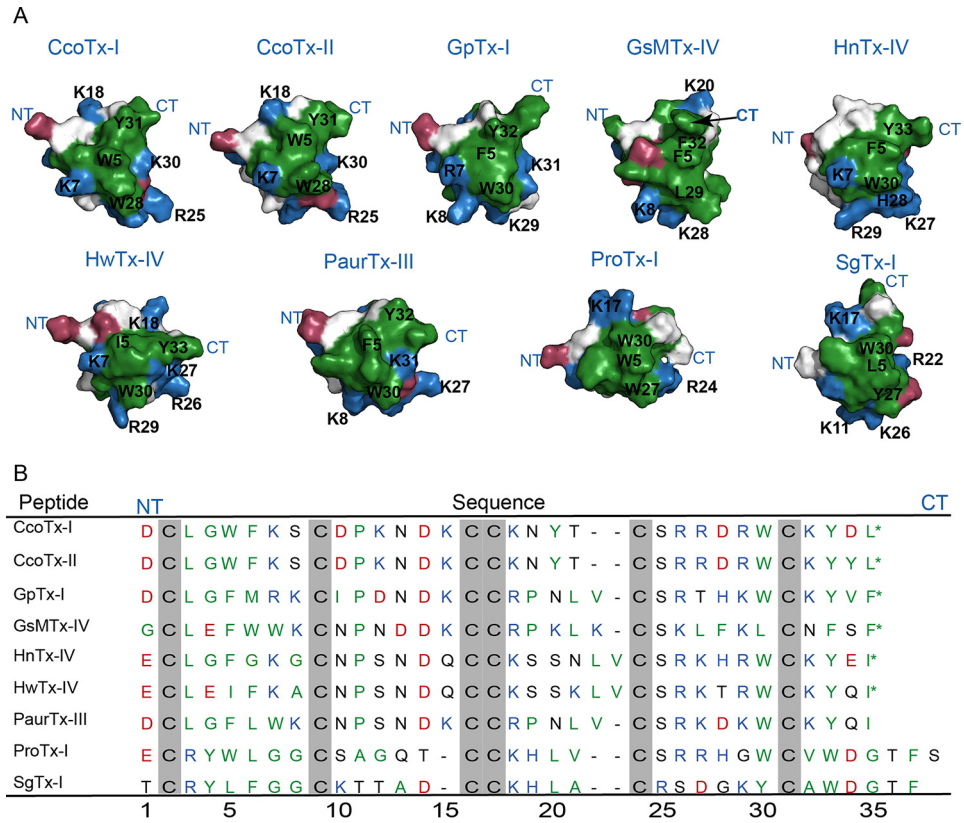

Figure 1. Surface profiles and sequences of the panel of nine GMTs used in this study. Shown are CcoTx-I (PDB code 6BR0), CcoTx-II (PDB code 6BTV), GpTx-I (23), HnTx-IV (PDB code 1NIY) (21), HwTx-IV (PDB code 2M4X) (29), PaurTx-III (PDB code 5WE3) (33), ProTx-I (PDB code 2M9L) (30), and SgTx-I (PDB code 1LA4) (32). *A*, *surface representations* of the GMTs *colored* by residue type: hydrophobic (*green*), positively charged (*blue*), negatively charged (*red*), and uncharged (*white*). All of the peptides are in the same orientation. *B*, alignment of GMT sequences relative to HnTx-IV and HwTx-IV. Cysteine residues are *highlighted* in *gray*. Residues that contribute to the hydrophobic patch (*green*) and positively charged ring (*blue*) as well as negatively charged residues (*red*) are *labeled*. *NT* and *CT*, N and C termini of the peptides, respectively. *, C-terminal amidation (residue numbers are shown *below* the *table*).

tivity. Previous reports have examined lipid-binding properties of small GMT cohorts (10, 11, 17, 18), but the current study represents the first concerted effort to study the membrane binding of a cohort of native GMTs in model membranes chosen to mimic physiological properties (15).

CcoTx-I, CcoTx-II, PaurTx-III, and ProTx-I were chosen because these GMTs are known promiscuous modulators of Na_Vs (19, 20) and would therefore provide information on the relationship between GMT amphipathicity, promiscuity for Na_Vs, and affinity for lipid bilayers. HnTx-IV, HwTx-IV, and GpTx-I were chosen for their known potency at $Na_V1.7$ (21–23), and although we have recently examined the lipid affinity of HwTx-IV (24), we have not done so in the context of a comparative analysis with native GMTs. GsMTx-IV is a known modulator of stretch-activated mechano-sensitive channels with a mechanism of action that is primarily related to interactions with the lipid bilayer (12, 25) and was included in the present study as a positive control for the lipid affinity studies and as a negative control for the studies on Na_Vs. SgTx-I is a known modulator of K_V channels and is an inhibitor of the voltage of inactivation of $Na_V1.2$ (26–28) and, like GsMTx-IV, was included as a negative control for the studies on Na_Vs. Our results suggest that the conserved amphipathic surface profile of spider-derived GMTs is most probably an adaptation that allows the concomitant modulation of several voltage-gated ion channels and that GMTs have preferential affinity for anionic model membranes.

Results

Oxidative folding of GMTs

To optimize the yield of GMTs with correct disulfide connectivity, each peptide was subjected to 3–5 oxidative folding trials in which the effects of temperature and folding buffer were examined (pH was always 7.7–8.0) (Table S1). Peptide folding was monitored using analytical reverse-phase HPLC (RP-HPLC) and LC/MS (Fig. S1 and Table S1) Most GMTs were successfully folded at 25 °C in buffer containing 7.5% (v/v) acetonitrile (ACN) (method A). GsMTx-IV was folded using both method A and B but formed aggregates using method B, probably because of the lack of organic solvent (Table S1). Furthermore, oxidation using method B took 24 h for GsMTx-IV compared with 16 h for method A. Formation of disulfide bonds of both HnTx-IV and HwTx-IV proceeded in the absence of organic solvent at room temperature in 16 h (methods C and D), whereas SgTx-I and ProTx-I required a slow reaction in 0.1 M ammonium acetate buffer, using 2 M urea at 4 °C for 72 h (method E).

NMR analysis of the GMTs

One-dimensional ^1H spectra (Fig. S2) of all GMTs revealed good dispersion of amide-proton resonances (7–10 ppm), suggesting that the peptides were folded and structured. Hα chemical shifts derived from two-dimensional TOCSY and NOESY

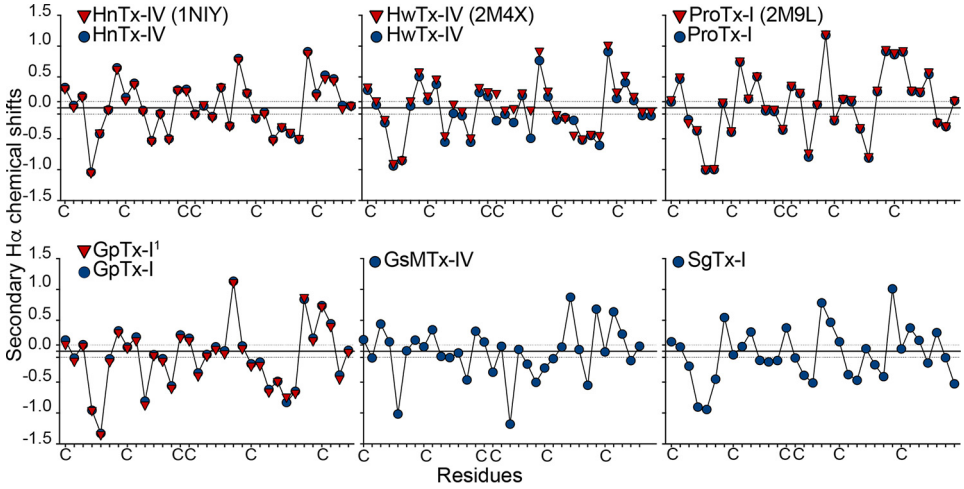

Figure 2. NMR analysis of GMTs included in this study. Secondary Hα chemical shifts of synthetic GMTs were obtained using 2D TOCSY and NOESY spectra. Secondary Hα chemical shifts were in agreement with literature shifts for HnTx-IV (PDB code 1NIY) (21), HwTx-IV (PDB code 2M4X) (29), ProTx-I (PDB code 2M9L) (30), and GpTx-I. *Superscript 1*, Hα shifts from Ref. 23.

spectra were used for sequential assignment of the peptides (Fig. 2), and Hα shifts for GpTx-I (23), HnTx-IV (PDB code 1NIY) (21), HwTx-IV (PDB code 2M4X), (29), and ProTx-I (PDB code 2M9L) (30) were in good agreement with literature values, with small differences attributable to differences in chemical shift referencing or pH (Fig. 2). Structures of GsMTx-IV and SgTx-I are available (31, 32), but Hα shifts have not been reported (Fig. 2). The solution structures and chemical shift assignments for CcoTx-I (PDB code 6BR0; BMRB 30376) and CcoTx-II (PDB code 6BTV; BMRB 30377) are reported here for the first time and have been submitted to the Protein Data Bank and to the BioMagnetic Resonance Bank, respectively (Fig. 3*A* and Table S2). The disulfide bridges in these GMTs form a classical inhibitory cystine knot motif in which the cystine knot stabilizes a structure composed of loops, turns, and two antiparallel β strands (Tyr^{20}–Cys^{22} and Cys^{29}–Tyr^{31}). The hydrophobic residues form a cluster with the side chains showing π–π stacking and attractive hydrophobic interactions (Fig. 3*B*). The structure for PaurTx-III, which we recently solved and submitted to the PDB (PDB code 5WE3; BMRB 30317) is also shown (Fig. 3) (33).

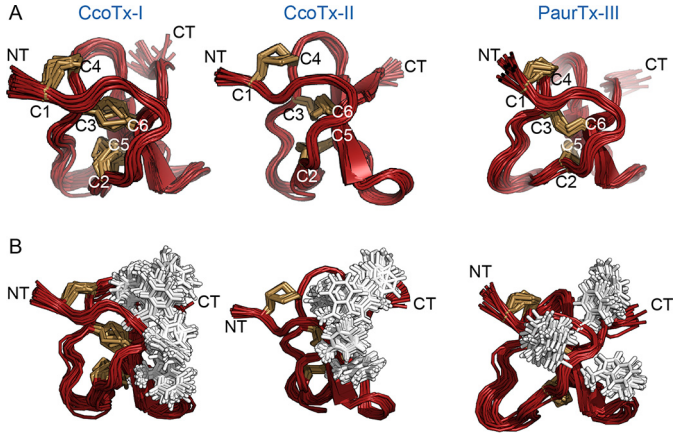

Figure 3. Solution NMR structure calculations of CcoTx-I (PDB code 6BR0), CcoTx-II (PDB code 6BTV), and PaurTx-III (PDB code 5WE3). Overlay of the ensemble of 20 conformers was selected on the basis of lowest energy of minimization and best MolProbity scores. *A*, *schematic* of CcoTx-I, CcoTx-II, and PaurTx-III with disulfide bridges shown in *gold* and cysteines *labeled*. NT and CT, N and C termini, respectively. *B*, the three GMTs are oriented the same way as in *A* with side chains of aromatic residues forming the hydrophobic patch shown in *white*.

GMT–lipid bilayer interactions

Surface plasmon resonance (SPR) was used to compare GMT affinity for different model membranes. Comparisons are made relative to GsMTx-IV, which had the highest affinity for all of the model membranes (Fig. 4 and Table S3). Within the context of the current study, affinity refers to amount of peptide bound to lipid (peptide/lipid (P/L) (mol/mol)) and the rate of dissociation of the peptide from the lipid bilayer (Fig. 4 and Table S3). Here, "weak affinity" refers to GMTs that either dissociate from the lipid bilayers rapidly or do not reach a P/L (mol/mol) that is as high as GsMTx-IV. In some instances, we compare the affinity of specific GMTs with different model membranes, in which case "weak affinity," "high affinity," or "preferential affinity" compares a specific peptide's affinity for one model membrane with another model membrane.

Our examination of GMT interactions with model membranes began with lipid bilayers composed of zwitterionic 1-palmitoyl-2-oleoyl-*sn*-glycero-3-phosphocholine (POPC), as phospholipids containing phosphatidylcholine headgroups are the most abundant phospholipids in the outer leaflet of healthy mammalian cells (34). Sensorgrams and concentration-response curves revealed that GsMTx-IV had the highest affinity (highest amount of maximum peptide bound to lipid (*i.e.* 0.071 P/L (mol/mol)) with the slowest dissociation from the POPC model membranes) (Fig. 4 and Table S3). The remaining peptides had weak affinity (0.002–0.031 P/L (mol/mol)) for POPC lipid bilayers (Fig. 4 and Table S3).

There is evidence that voltage-gated ion channels are embedded within lipid rafts that form domains around these transmembrane proteins for functional and structural integrity (35, 36). A mixture of POPC/sphingomyelin (SM)/cholesterol (CHOL) (2.7:4:3.3 molar ratio) was therefore used to mimic the environment formed by lipid rafts (37, 38). GsMTx-IV and CcoTx-II showed the highest amount of peptide bound to lipid (0.045 and 0.041 P/L (mol/mol), respectively), although

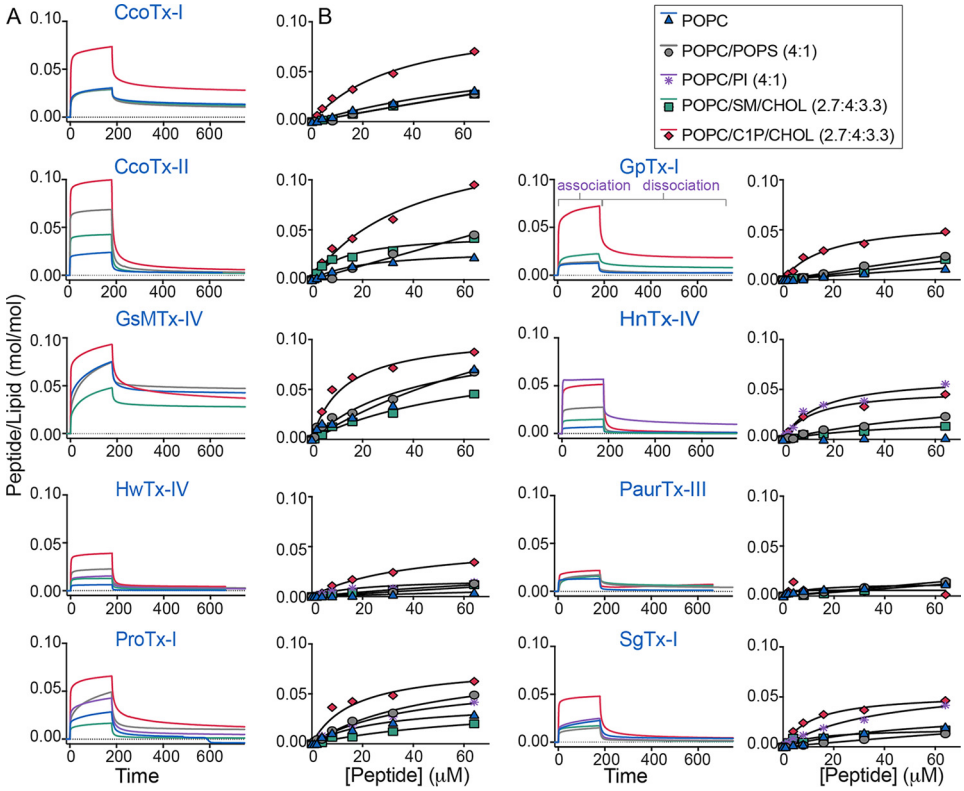

Figure 4. Binding of GMTs to model membranes. *A*, SPR sensorgrams of each peptide at 64 μM. *B*, corresponding concentration–response curves were obtained and used to examine the affinity of GMTs for model membranes composed of POPC, POPC/POPS (4:1), POPC/SM/CHOL (2.7:3.3:4), and POPC/C1P/CHOL (2.7:3.3:4). For HnTx-IV, HwTx-IV, ProTx-I, and SgTx-I, POPC/PI (4:1) model membranes were also examined. Peptide association and dissociation phase are indicated on the sensorgram for GpTx-I. Response units were converted to ratio of peptide/lipid (mol/mol) at the end of peptide injection (t = 170 s), and concentration–response curves were obtained using peptide concentrations ranging from 0 to 64 μM.

CcoTx-II dissociated faster than GsMTx-IV. All other peptides bound weakly to POPC/SM/CHOL model membranes (0.012–0.028 P/L (mol/mol)) (Fig. 4 and Table S3).

We also examined GMT affinity for anionic POPC/ceramide 1-phosphate (C1P)/CHOL (2.7:4:3.3) model membranes, in which C1P possesses a negatively charged headgroup. It was previously shown that GMTs have stronger affinity for voltage-gated ion channels when sphingomyelinase D (SMase D), an enzyme found in the venom of sicariid spiders, hydrolyzes SM to C1P (35, 36, 38). The GMTs had the highest affinity for this model membrane compared with other model membranes used in this study except for PaurTx-3, which showed weak affinity for this lipid type (0.001 P/L (mol/mol)) (Fig. 4 and Table S3).

We also examined GMT affinity for POPC/1-palmitoyl-2-oleoyl-*sn*-glycero-3-phospho-L-serine (POPS) (4:1) model membranes because phosphatidylserine phospholipids have frequently been used to mimic the influence of anionic moieties found on the outer leaflet of cell membranes (11, 24, 38, 39). CcoTx-II, HnTx-IV, ProTx-I, and HwTx-IV showed preferential binding to POPC/POPS (4:1) over POPC lipid bilayers (0.045, 0.023, 0.049, and 0.013 P/L (mol/mol), respectively, for POPC/POPS compared with 0.023, 0.002, 0.029, and 0.004 P/L (mol/mol), respectively, for POPC). However, there was no difference between binding to POPC and POPC/POPS (4:1) for CcoTx-I, GsMTx-IV, GpTx-I, and SgTx-I (Fig. 4 and Table S3).

Phosphatidylinositol phospholipids are negatively charged; they form a ringlike shell around transmembrane proteins and may have a role in modulating the function of voltage-gated ion channels (37, 40, 41). Thus, we examined the affinity of HnTx-IV, HwTx-IV, ProTx-I, and SgTx-II for model membranes composed of POPC/L-α- phosphatidylinositol (PI) (4:1). HnTx-IV had the highest amount of peptide bound to model membrane (0.055 P/L (mol/mol)) but dissociated rapidly (Fig. 4), whereas HwTx-IV had the lowest affinity (0.015 P/L (mol/mol)). The four peptides bound to POPC/PI with higher affinity than their binding to POPC lipid bilayers (0.055, 0.015, 0.042, and 0.042 P/L (mol/mol) for HnTx-IV, HwTx-IV, ProTx-I, and SgTx-I, respectively, at POPC/PI compared with 0.002, 0.004, 0.029, and 0.020 P/L (mol/mol), respectively, for POPC) (Fig. 4 and Table S3).

GMT interactions with model membranes upon variation of ionic strength

To examine the importance of electrostatic interactions in driving GMT binding to model membranes, we compared GMT binding to POPC/POPS (4:1) lipid bilayers in buffers of varying ionic strength. All GMTs showed increased binding to lipid vesicles formed in lower-ionic strength buffer (50 mM NaCl) compared with lipid vesicles formed in high-ionic strength buffer (300 mM NaCl) (Fig. 5). PaurTx-III, HnTx-IV, and GpTx-I had fast dissociation rates from lipid bilayers prepared in low ionic strength buffer, suggesting that these three GMTs form weaker electrostatic interactions with POPC/POPS (4:1) lipid bilayers than the remaining six GMTs (Fig. 5).

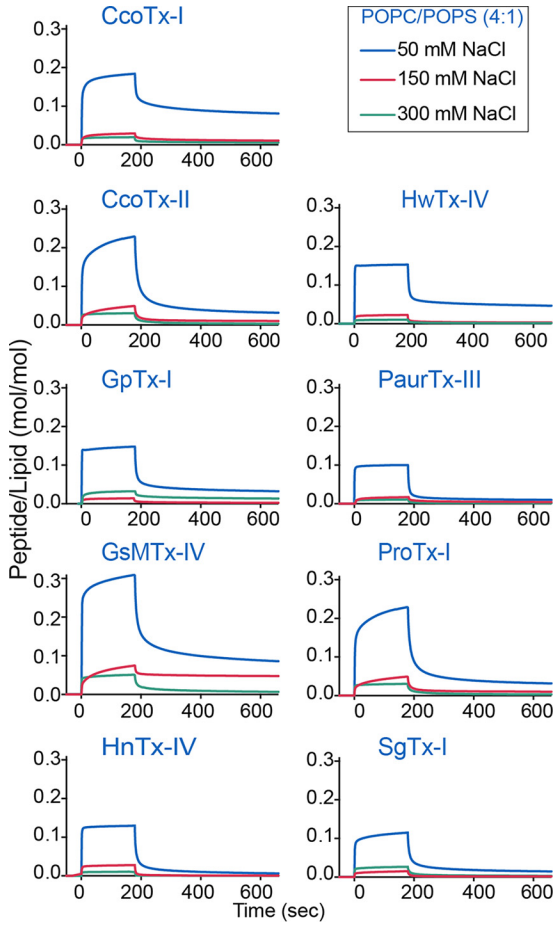

Figure 5. The importance of electrostatic forces in peptide–lipid interactions. Interactions of GMTs with POPC/POPS (4:1) bilayers prepared in buffers of different ionic strength (50, 150, or 300 mM NaCl) in 10 mM HEPES, pH 7.4, are shown.

Analysis of environment surrounding GMT Trp residues upon lipid titration

The fluorescence emission spectrum of Trp residues depends on their local environment. As a Trp residue on a peptide moves from a polar to an apolar environment, an increase in quantum yield and a leftward (blue) shift of the fluorescence emission spectrum is expected (42, 43). These properties were used to examine whether Trp residues found on GMTs insert into the hydrophobic acyl chains of model membranes. Large unilamellar vesicles (LUVs) were used to mimic a planar bilayer surface (42, 44). All nine GMTs have a fluorescence emission spectrum with a maximum near 350 nm, which is close to the fluorescence emission of L-Trp in buffer (354 nm), suggesting the presence of solvent-exposed Trp residues and that the fluorescence spectra can be used to gauge whether the peptides move from a polar to an apolar environment. None of the GMTs showed a significant change in the fluorescence emission properties of their Trp residues upon titration with POPC/POPS LUVs (Fig. 6), suggesting that the Trp residues do not deeply insert into the acyl core of the lipid bilayers but rather adopt a superficial position on the lipid bilayer. The conclusion that the peptides adopt a shallow position is supported by the SPR data for the peptide affinity at POPC/POPS model membranes (Fig. 4). In this assay, none of the peptides bound to the lipid at a ratio of >0.1 P/L (mol/mol), which suggests that the peptides did not insert deeply into the lipid bilayer. For comparison, [E5K,E8K]MfVIA, a peptide that we have recently reported on, showed both an increase in quantum yield and a blue shift in the emission spectrum (Fig. 6), accompanied by a maximum P/L mol/mol ~0.5, as calculated using SPR in the presence of POPC/POPS model membranes (45).

Inhibitory potency of GMTs at $Na_V1.7$

GMT inhibition of $Na_V1.7$ current was examined using whole-cell patch-clamp electrophysiology. All peptides except for SgTx-I and GsMTx-IV inhibited $Na_V1.7$ with mid-nanomolar potency, as reported for ProTx-I, GpTx-I, and HwTx-IV (19, 23, 46). HnTx-IV was the most potent inhibitor of $Na_V1.7$, followed by ProTx-I, HwTx-IV, PaurTx-III, CcoTx-II, GpTx-I, and CcoTx-I in descending order of potency (Fig. 7).

Na_V subtype selectivity of GMTs

Two-electrode voltage-clamp electrophysiology was used to examine the effect of GMTs on $Na_V1.2$, $Na_V1.4$, $Na_V1.5$, and $Na_V1.6$ expressed in *Xenopus* oocytes (difficulties with expression of $Na_V1.7$ in oocytes precluded two-electrode voltage clamp studies). The GMTs showed an absence of selectivity when studied against the Na_V channels (Fig. 8 and Table 1). ProTx-I, CcoTx-I, PaurTx-III, and CcoTx-II inhibited 80-100% of current from all of the Na_V channels examined (Fig. 8 (*A–D*) and Table 1). HwTx-IV, HnTx-IV, and GpTx-I had the best overall selectivity, as they only showed complete current inhibition of $Na_V1.2$ and $Na_V1.6$ but did not completely inhibit current from $Na_V1.4$ and $Na_V1.5$, as seen for CcoTx-I, CcoTx-II, PaurTx-III, and ProTx-I (Fig. 8 and Table 1). HwTx-IV was equipotent on $Na_V1.2$ and $Na_V1.6$ (Fig. 8 and Table 1), whereas HnTx-IV was slightly more potent at $Na_V1.2$ and had 2-fold lower potency for $Na_V1.6$ (Fig. 8 and Table 1). GpTx-I had the best overall selectivity, with a 6-fold difference in potency between $Na_V1.6$ and $Na_V1.2$ (Fig. 8 and Table 1). GsMTx-IV failed to inhibit 100% of current from any Na_V channel subtype, and SgTx-I caused a delay in channel inactivation accompanied by an increase in sodium peak current. Despite these differences between GsMTx-IV and SgTx-I compared with the remaining seven GMTs, both GsMTx-IV and SgTx-I were not selective (Fig. 8 and Table 1).

Examination of the physicochemical properties of the GMTs

All nine GMTs have similar net positive charge with no observable relationship between net charge and affinity for lipid membranes (Table 2 and Fig. 9*A*). GMT hydrophobicity was compared using their RP-HPLC retention times, and the proportion of apolar solvent-accessible surface area (SASA) was used to measure the solvent-accessible hydrophobic area of each peptide. There was no correlation between GMT hydrophobicity or apolar SASA and membrane binding (Table 2 and Fig. 9 (*B* and *C*)). For instance, CcoTx-I and PaurTx-III have retention times of ~27 min and apolar SASAs of 57 and 65%, respectively, but these peptides show different affinities for the lipid bilayers examined (Table 2 and Figs. 4 and 9). Likewise, PaurTx-III and GsMTx-IV have the highest percentage of apolar SASAs (65 and 66%, respectively) but consistently had the

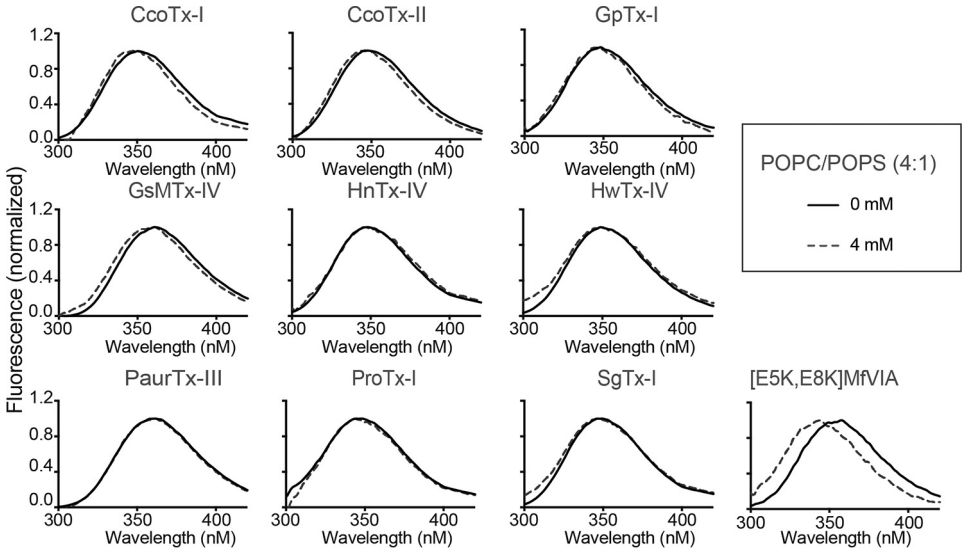

Figure 6. Analysis of the environment around GMT Trp residues upon lipid titration. Fluorescence emission spectra of the peptides were followed in the absence (0 mM) and presence (4 mM) of POPC/POPS (4:1) LUVs. Excitation was at $\lambda = 280$ nm; peptide concentrations were 25 μM for all GMTs except PaurTx-III (12.5 μM) in HEPES-buffered saline. Spectra for [E5K,E8K]MfVIA, are included as a positive control (45).

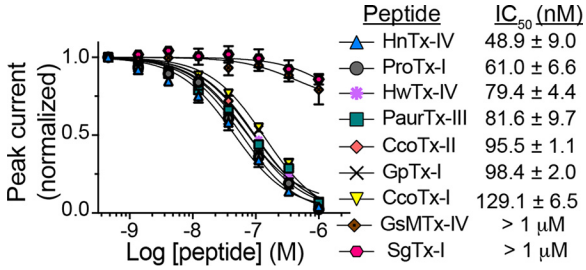

Figure 7. GMT inhibition of $Na_V1.7$. Automated whole-cell patch-clamp electrophysiology was used to compare the inhibitory potency of the peptides at $Na_V1.7$. Representative concentration–response curves and comparative IC_{50} values for the peptides are shown. Data are mean ± S.E. (*error bars*), where $n = 3$ and one cell was considered an independent experiment.

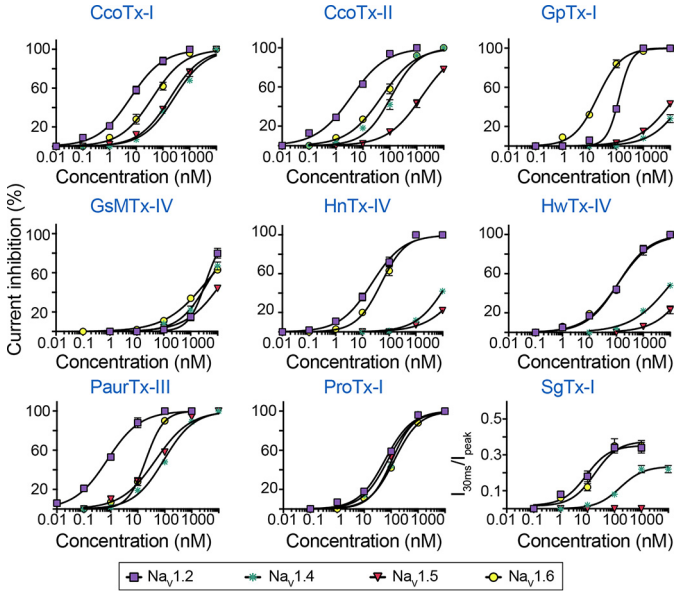

Figure 8. Na_V subtype selectivity of GMTs. Two-electrode voltage clamp electrophysiology on oocytes was used to examine the effects of GMTs $Na_V1.2$, $Na_V1.4$, $Na_V1.5$, and $Na_V1.6$. All GMTs promiscuously modulated the activity of all Na_V channels tested, with GpTx-I, HwTx-IV, and HnTx-IV showing the best overall selectivity. SgTx-I showed an increase in current influx for Na_V channel subtypes; therefore, $I_{30\ ms}/I_{peak}$ is shown for this peptide. Data for the remaining eight peptides were normalized to maximum current inhibition. *Error bars*, S.E., where $n = 3$.

weakest and strongest affinities, respectively, for the model membranes studied (Table 2 and Figs. 4 and 9).

Discussion

GMTs isolated from spider venom share a conserved hydrophobic patch surrounded by a ring of positively charged residues that together have been proposed to promote peptide affinity for lipid membranes (Fig. 1) (8, 47). Here, we examined the extent to which nine GMTs bound to a series of model membranes, whether there is a relationship between membrane binding and inhibition of $Na_V1.7$, and whether GMT amphipathicity is important for membrane binding and/or inhibition of Na_V channels.

GMT affinity for model lipid bilayers

Overall, the nine GMTs showed weak affinity for model membranes prepared using POPC and mixtures of POPC/SM/CHOL (Fig. 4 and Table S3), in agreement with previous studies showing that GMTs such as VsTx-I, Hd1a, and ProTx-II have weak affinity for zwitterionic model membranes (8, 13, 17, 24, 38, 39, 46).

GMTs showed preferential affinity for negatively charged POPC/C1P/CHOL model membranes compared with those made from POPC/SM/CHOL (Fig. 4 and Table S3), as observed previously for ProTx-II (38). Interestingly, the pharmacology of some voltage-gated ion channels has previously shown sensitivity to the enzymatic conversion of SM to C1P by SMase D (35, 36); it is possible that sicariid spiders take advantage of the presence of SMase D, and perhaps additional venom components, to increase GMT binding to both cell membranes and the voltage-gated ion channels to optimize activity (38). This hypothesis is supported by a study showing that ProTx-I has increased affinity for voltage-gated ion channels upon conversion of SM to C1P by SMase D (36).

Table 1
Gating modifier toxin inhibition of voltage-gated sodium channels
Percentage inhibition of sodium currents was measured using TEVC electrophysiology, and EC_{50} values are mean ± S.E. ($n = 3$).

Peptide	EC_{50}			
	$Na_V1.2$	$Na_V1.4$	$Na_V1.5$	$Na_V1.6$
	nM			
ProTx-I	59.7 ± 7.4	108.6 ± 19.3	76.3 ± 9.1	133 ± 10
CcoTx-I	6.1 ± 0.7	263 ± 45	188 ± 20	40.6 ± 5.8
PaurTx-III	0.70 ± 0.07	92.9 ± 12.7	46.3 ± 8.8	20.0 ± 2.1
CcoTx-II	3.7 ± 0.6	113 ± 24	1524 ± 58	49.9 ± 7.1
GsMTx-IV	>3 μM	>3 μM	>10 μM	>3 μM
SgTx-I[a]	>3 μM	>10 μM	>10 μM	>3 μM
HwTx-IV	116 ± 16	>10 μM	>10 μM	117 ± 21
HnTx-IV	22.4 ± 3.0	>10 μM	>10 μM	50.1 ± 7.4
GpTx-I	128 ± 12	>10 μM	>10 μM	20.1 ± 1.7

[a] Values for SgTx-I are $I_{30\ ms}/I_{peak}$ because this GMT displayed a delay in channel inactivation accompanied by an increase in current.

Table 2
Physicochemical properties of GMTs

Peptide	Peptide RT[a]	Polar SASA[b]	Apolar SASA	Percentage of Apolar SASA	Net charge[c]
	min			*%*	
CcoTx-I	26.5	1230	1653	57	3
CcoTx-II	27.0	1083	1736	62	4
GpTx-I	24.1	1187	1873	61	4
GsMTx-IV	35.4	1023	2010	66	5
HnTx-IV	20.7	1245	1604	56	4
HwTx-IV	26.0	1289	1888	59	4
PaurTx-III	26.9	1046	1914	65	4
ProTx-I	32.7	1165	1830	61	2
SgTx-I	35.7	1001	1823	65	2

[a] Retention time of peptides obtained by analytical HPLC (1%/min gradient of 0–60% solvent B at a flow rate of 0.3 ml/min).
[b] SASA calculated using GETAREA: http://curie.utmb.edu/getarea.html. (Please note that the JBC is not responsible for the long-term archiving and maintenance of this site or any other third party hosted site.)
[c] Net charge was calculated at pH 7.4 using pK_a values from Propka (jensengroup) (59).

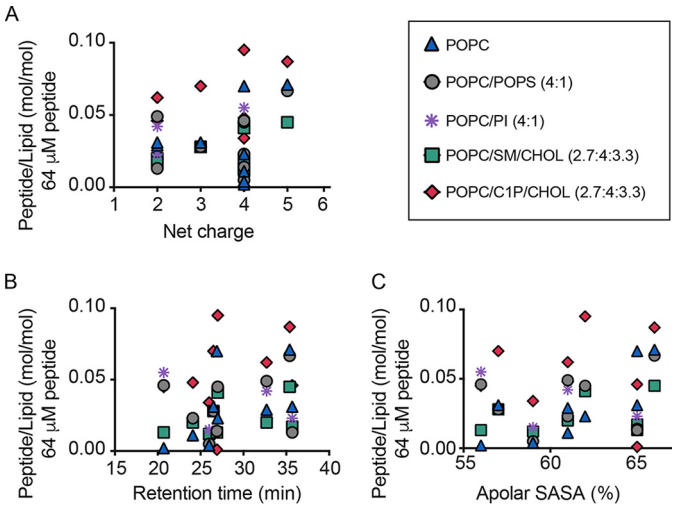

Figure 9. No correlation between membrane binding (peptide/lipid mol/mol) and apolar surface area (*A*), net charge (*B*), and hydrophobicity (*C*) as measured by retention time on analytical RP-HPLC. Each *symbol* represents a lipid system and the quantitative physicochemical value of the peptides in the present study.

The preferential affinity of GMTs for anionic compared with zwitterionic model membranes was further observed in a higher GMT affinity for POPC/POPS and POPC/PI compared with POPC lipid bilayers (Fig. 4). This affinity is presumably driven by electrostatic interactions between the positively charged peptides and anionic lipid headgroups and may be indicative of GMT affinity for negative moieties on the outer leaflet of cell membranes (Table 2). The importance of electrostatic interactions is further supported by the observed increase in GMT affinity for POPC/POPS with low ionic strength (see results with 50 mM NaCl; Fig. 5). These results agree with previous studies that also emphasized the importance of electrostatic interactions in driving GMT binding to lipid bilayers (10, 18, 38, 39).

Analysis of the environment surrounding GMT Trp residues in anionic lipids

The absence of a blue shift or change in quantum yield in the fluorescence spectra of the GMTs in the presence of anionic lipids (Fig. 6) suggests that they adopt a shallow position on anionic lipid bilayers as reported for ProTx-II and ProTx-I (38, 39). Although SgTx-I and HaTx-I were previously shown to insert into lipid membranes up to a distance of ~9 Å from the center of the bilayer, these studies employed model membranes containing 50% anionic PG-phospholipids, and model membranes were prepared in solutions without NaCl (9, 48). Some GMTs like VsTx-I modulate the function of bacterial voltage-gated potassium channels (3, 13, 49); therefore, the use of PG-phospholipids can be justified in the studies of the trimolecular complex formed by these peptides. However, PG-phospholipids are unlikely to be found on the outer leaflet of mammalian cell membranes (34) and therefore were not included in the current study. Taken together, the present work indicates that GMTs adsorb to the outer leaflet of anionic lipid bilayers.

Relationship between GMT–membrane binding and Na_V channel inhibition

Potency of the panel of GMTs for $Na_V1.7$ appears not to be correlated to affinity for any model membrane. For example, GsMTx-IV and SgTx-I are both known poor inhibitors of $Na_V1.7$ but had different affinities for the model membranes. The other GMTs studied were mid-nanomolar inhibitors of $Na_V1.7$ (Fig. 7) but had varied affinities for the model membranes. We previously showed that reducing the membrane affinity of ProTx-II results in analogues with weaker potency at $Na_V1.7$ (38). We also demonstrated that the membrane binding and potency of HwTx-IV can be increased without changing the pharmacophore of this particular GMT (24). Thus, although membrane binding is not essential for inhibition of $Na_V1.7$, modulating affinity of individual GMTs for lipid bilayers can be exploited to increase or decrease potency.

We next examined whether differences in membrane binding properties might be important in dictating Na_V subtype selectivity. None of the GMT studied displayed exceptional selectivity for any Na_V channel subtype (Fig. 8 and Table 1), affirming previous reports on the promiscuity of most of these peptides (14, 19, 20). There was also no direct correlation between selectivity and membrane binding. However, GpTx-I, HwTx-IV, and HnTx-IV, three peptides with an overall weak affinity for model membranes in the current study (Fig. 4), had the best overall selectivity, as they achieved 100% current inhibition and strong potency only for $Na_V1.2$ and $Na_V1.6$ (Fig. 8). Conversely, ProTx-I, CcoTx-I, and CcoTx-II, three peptides that achieved 100% current inhibition for at least three Na_V chan-

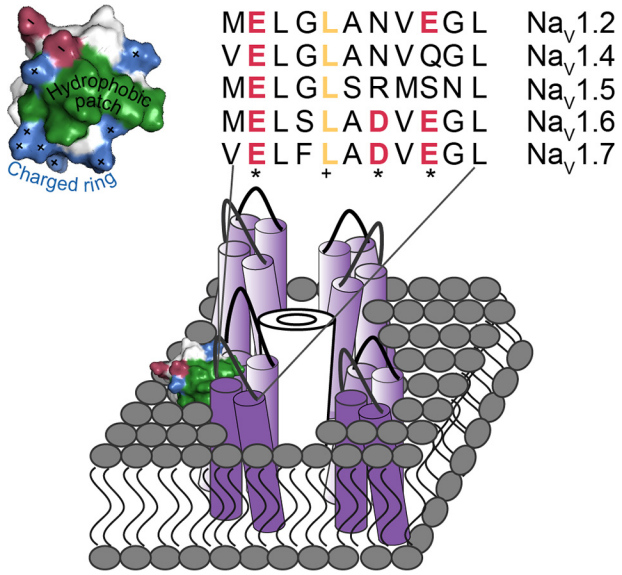

Figure 10. The hydrophobic patch and surrounding cationic ring in spider venom GMTs promotes Na_V channel promiscuity. HnTx-IV (PDB code 1NIY) is shown as a representative GMT with hydrophobic patch (*green*), positively charged residues (*blue*), and anionic amino acid residues (*red*). A *cartoon representation* of a Na_V channel is shown (adapted from Ref. 24), with the putative GMT target sequences of $Na_V1.2$, $Na_V1.4$, $Na_V1.5$, $Na_V1.6$, and $Na_V1.7$ also shown to highlight the conserved hydrophobic amino acid residues (*boldface yellow type* with *cross below*) and anionic amino acid residues (*boldface red type* with *asterisk below*).

nel subtypes (Fig. 8 and Table 1), all had overall higher affinity for model membranes compared with HnTx-IV, HwTx-IV, and GpTx-I (Fig. 5). Therefore, it appears that increasing membrane binding is unlikely to improve the Na_V subtype selectivity of spider venom GMTs.

Deductions on the role of GMT amphipathicity in Na_V inhibition

There was also no apparent correlation between GMT physicochemical properties and affinity for the lipid membranes studied (Fig. 9), and these results are in agreement with our previous work involving a smaller sample of GMTs (39). Because the global physicochemical properties of native GMTs are not correlated with their propensity to interact with cell membranes, and there is no correlation between membrane binding and the modulation of Na_V channels, the combination of a hydrophobic patch and positively charged ring is a conserved feature more likely to promote simultaneous potency for several voltage-gated channels. The current consensus is that GMTs employ certain residues incorporated in the hydrophobic patch and positively charged ring to bind to conserved sequences consisting of hydrophobic and anionic amino acid residues on voltage-gated ion channels (Fig. 10) (23, 29, 46, 50–52). This hypothesis is supported by two observations: (i) the overall potency of most GMTs is comparatively lower for $Na_V1.4$, $Na_V1.5$, or both (Fig. 8), and these channels have fewer anionic residues in the GMT binding region of their voltage-sensor domains (Fig. 10); (ii) SgTx-I and GsMTx-IV, which either have a different mechanism of action or do not potently inhibit Na_Vs, respectively (Fig. 8), have fewer positively charged residues in their C-terminal regions (Fig. 1*B*). The C-terminal region contains residues that contribute to the putative pharmacophores of some GMTs that inhibit Na_V channels, including HnTx-IV, HwTx-IV, and GpTx-I for $Na_V1.7$ (23, 29, 53).

Conclusions and summary

This study revealed that some GMTs adsorb via electrostatic interactions to the outer leaflet of anionic lipid membranes and that the amphipathic surface profile of the peptides is most probably an adaptive strategy that enables simultaneous inhibition of several voltage-gated ion channels (Fig. 10), in a multipronged approach to immobilize insect prey (54). From a pharmacological perspective, application of the trimolecular complex to rational drug design cannot be based on broad generalizations about GMTs, but each GMT will require focused studies to explore the possibilities that membrane interactions present.

Most studies on the trimolecular complex have thus far been limited by distinct studies of GMT–model membrane and GMT–ion channel interactions. However, as novel systems continue to be developed, including the use of nanodiscs containing the transmembrane voltage-gated ion channels in combination with rationally chosen model membranes, techniques such as cryo-EM and NMR might be able to provide better insights into the tripartite interactions occurring between GMTs, lipids, and the voltage-gated ion channels (13, 15, 55).

Experimental procedures

Peptide synthesis and folding

GMTs were synthesized using Fmoc (*N*-(9-fluorenyl)methoxycarbonyl) chemistry and purified as described previously (24, 38). Briefly, peptides were assembled on a 2-chlorotrityl chloride resin or on a Rink amide resin if C-terminal amidation was required (Fig. 1*B*). All peptides were synthesized at a scale of 0.25 mmol on a Symphony peptide synthesizer (Gyros Protein Technologies, Tuscon, AZ). Peptides were released from resin, and side-chain protecting groups were simultaneously removed by treatment with 96% (v/v) TFA, 2% (v/v) H_2O, and 2% (v/v) triisopropylsaline for 2.5 h. Cleaved, reduced peptides were purified using RP-HPLC on a C18 column (Phenomenex Jupiter, 250 × 50 mm, 10 μm; Phenomenex, Torrance, CA), using a 1%/min gradient of 0–50% solvent B (solvent B: 90% (v/v) ACN and 0.05% (v/v) TFA) in solvent A (0.05% (v/v) TFA), and peptide elution was monitored at 215 and 280 nm. Electrospray ionization-MS was used to identify relevant fractions, which were pooled and lyophilized before oxidative folding of the peptides.

Optimal conditions for oxidative folding of GMTs were chosen from one of several buffer formulations (Table 1). In each case, peptides were added into the oxidation buffer dropwise to achieve a final peptide concentration of 0.1 mg/ml and oxidized at 25 °C unless otherwise stated. CcoTx-I, CcoTx-II, GpTx-I, GsMTx-IV, and PaurTx-III were dissolved in 50% (v/v) ACN and added to a buffer containing 7.5% (v/v) ACN and 0.1 M Tris, 0.81 mM GSH, and 0.81 mM GSSG at pH 7.7. Reactions were quenched by lowering the solution to pH 4 after 16 h using 2 M acetic acid (method A) (23). GsMTx-IV was also successfully oxidized by dissolving the peptide in 50% (v/v) ACN and adding it to 0.1 M Tris, 10 mM GSH, and 1 mM GSSG at pH 7.8. The reaction was quenched by lowering the solution to pH 2 after

24 h using 100% (v/v) TFA (method B) (56). HnTx-IV was oxidized using 0.1 M Tris, 0.1 M NaCl, 5 mM GSH, and 0.5 mM GSSG at pH 8. 100% (v/v) HCl was used to quench the reaction to pH 4 after 16 h (method C) (53). HwTx-IV was oxidized using 0.1 M Tris, 5 mM GSH, and 0.5 mM GSSG, pH 8. The reaction was quenched after 16 h to pH 4 using 100% (v/v) HCl (method D) (46). ProTx-I and SgTx-I were oxidized at 4 °C in 0.1 M ammonium acetate, 2 M urea, 2.5 mM GSH, and 0.25 mM GSSG. pH was adjusted to 7.8 using ammonium solution. The reactions were quenched after 72 h by lowering the buffer solution to pH 3 using 2 M acetic acid (method E) (32). All oxidation reactions were monitored using LC/MS and analytical RP-HPLC (1%/min gradient of 0–60% solvent B at a flow rate of 0.3 ml/min) using a C18 analytical column (Grace Vydac, 150 × 2.1 mm, 5 μm; Thermo Fisher Scientific, Waltham, MA).

Folded peptides were purified via RP-HPLC using a preparatory C18 column (Agilent, 250 × 30 mm, 100 Å; Agilent Technologies) with a 1%/min gradient of 10–70% solvent B at a flow rate of 8 ml/min and further using a semipreparatory C18 column (Phenomenex Gemini, 250 × 10 mm, 5 μm) at 3 ml/min on a 0.5%/min gradient of 15–45% solvent B. Relevant fractions were pooled, lyophilized, and stored at −20 °C. Folding of the peptides was confirmed using NMR spectroscopy.

NMR spectroscopy

Peptides were dissolved to a concentration of ~1 mg/ml in 90% (v/v) H_2O and 10% (v/v) D_2O at pH 6. NMR spectra were collected at 25 °C on an Avance 600-MHz NMR spectrometer equipped with a cryoprobe (Bruker Biospin, Callerica, MA). NMR experiments, used to examine the structure of the peptides, included 1D ^{1}H and 2D TOCSY (80-ms mixing time) and NOESY (200-ms mixing time). Spectra were processed using TopSpin version 3.5 (Bruker), and resonances were assigned using CCPNMR Analysis version 2.4.1 (CCPN, University of Cambridge, Cambridge, UK) (57). The assigned Hα chemical shifts of GpTx-I (23), HnTx-IV (PDB code 1NIY), HwTx-IV (PDB code 2M4X), and ProTx-I (PDB code 2M9L) were consistent with previously published values (21, 29, 30).

Additional NMR spectra acquired to determine the solution structures of CcoTx-I and CcoTx-II included natural abundance 2D ^{1}H-^{15}N HSQC and ^{1}H-^{13}C HSQC (samples in 90% (v/v) H_2O and 10% (v/v) D_2O) and ^{1}H-^{1}H, TOCSY, NOESY, and E.COSY (samples in 100% (v/v) D_2O). A series of TOCSY spectra was obtained in 5 °C temperature increments (from 10 to 35 °C) to obtain amide proton temperature coefficients. The structures of the two peptides were calculated from the NMR data using methods described previously (24, 33). The structure of PaurTx-III (PDB code 5WE3) has recently been published (33).

Calculations of physicochemical properties

The SASA of each peptide was calculated with GETAREA (58), using a 1.4-Å water probe to compare polar and apolar surface areas of the peptides. Propka (Jensengroup) (59) was used to assign protonation states to the side chains at pH 7.4 for net charge calculations. Hydrophobicity was assumed to be directly proportional to retention time of the peptides when eluted using a 1%/min gradient of 0–60% solvent B at a flow rate of 0.3 ml/min on analytical RP-HPLC using a C18 column (Grace Vydac, 150 × 2.1 mm, 5 μm).

Peptide quantification

Peptide concentrations were determined from absorbance at 280-nm using theoretical extinction coefficients (ϵ_{280}) calculated from the sum of contributions from Trp amino acid residues (ϵ_{280} = 5690 $M^{-1}\cdot cm^{-1}$), Tyr amino acid residues (ϵ_{280} = 1280 $M^{-1}\cdot cm^{-1}$), and disulfide bonds (ϵ_{280} = 120 $M^{-1}\cdot cm^{-1}$) (60): CcoTx-I ϵ_{280} = 14300 $M^{-1}\cdot cm^{-1}$; CcoTx-II ϵ_{280} = 15,580 $M^{-1}\cdot cm^{-1}$; GpTx-I ϵ_{280} = 7330 $M^{-1}\cdot cm^{-1}$; GsMTx-IV ϵ_{280} = 11,740 $M^{-1}\cdot cm^{-1}$; HnTx-IV ϵ_{280} = 7330 $M^{-1}\cdot cm^{-1}$; HwTx-IV ϵ_{280} = 7365 $M^{-1}\cdot cm^{-1}$; PaurTx-III ϵ_{280} = 12,865 $M^{-1}\cdot cm^{-1}$; ProTx-I ϵ_{280} = 18,365 $M^{-1}\cdot cm^{-1}$; SgTx-I ϵ_{280} = 8610 $M^{-1}\cdot cm^{-1}$.

Preparation of lipid vesicles

Lipids used included CHOL (Sigma-Aldrich), PI (soy extract), POPC, POPS, C1P, and SM (Avanti Polar Lipids, Alabaster, AL). Molar ratio mixtures of the lipids were prepared in chloroform, the solvent was evaporated under a stream of N_2, and then lipids were dried overnight *in vacuo*. Lipid films were hydrated with buffer and lipid suspensions subjected to eight freeze-thaw cycles. Liposomes were then sized by extrusion through a polycarbonate filter (50 nm to produce small unilamellar vesicles (SUVs) or 100 nm for LUVs).

GMT–membrane interactions

SPR (Biacore 3000, GE Healthcare Life Sciences) was used to examine the binding of GMTs to model membranes made from molar ratio mixtures of POPC, POPC/POPS (4:1), POPC/PI (4:1), POPC/SM/CHOL (2.7:4:3.3), and POPC/C1P/CHOL (2.7:4:3.3). Unless otherwise stated, SUVs were prepared in HEPES buffer solution (10 mM HEPES, 150 mM NaCl, pH 7.4) and deposited on L1 sensor chips (2 μl/min, 2600 s). Peptides were injected at various concentrations (0–64 μM) over the lipid surface at a rate of 5 μl/min for 180 s; the dissociation phase was followed for 600 s. The effect of ionic strength on GMT affinity for lipid membranes was examined by comparing peptide binding to POPC/POPS (4:1) bilayers in 10 mM HEPES, pH 7.4, at varying concentrations of NaCl (50, 150, or 300 mM). The same buffer was used to prepare SUVs and peptide samples and as running buffer in SPR. All experiments were conducted at 25 °C. Binding affinity was compared by calculating the peptide/lipid ratio near the end of peptide injection and close to equilibrium (t = 170 s). Data were corrected for buffer contribution and normalized using the assumption that 1 response unit = 1 pg/mm^2 of lipid deposited (or peptide bound) (61). Concentration–response curves were fitted with a standard Hill equation using Prism version 7 (GraphPad Software Inc., La Jolla, CA). This is the first time we have reported on the current data for peptide–lipid affinity for CcoTx-I, CcoTx-II, GpTx-I, GsMTx-IV, HnTx-IV, PaurTx-3, and SgTx-I (Fig. 4); however, the data for peptide–lipid affinity for HwTx-IV as shown for POPC, POPC/POPS, POPC/SM/CHOL, and POPC/C1P/CHOL are in agreement with our recent study on HwTx-IV (Fig. 4 and Table S3) (24).

Fluorescence spectroscopy

Trp fluorescence emission spectra ($\lambda_{excitation}$ = 280 nm) of each GMT (25 μM, or 12.5 μM for PaurTx-III because the fluorescence emission spectrum for this GMT was saturated at 12.5 μM) were acquired upon titration with LUV suspensions (0–4 mM) to examine whether the environment surrounding the peptide Trp residue changes upon lipid titration (62). Data were corrected for dilution and light dispersion upon titration with vesicle suspension. The overall area of the emission spectra was used to compare quantum yield, and spectra were normalized to maximum fluorescence emission wavelength to check for presence of a blue shift. The fluorescence spectroscopy experiments for the eight peptides are represented here for the first time (Fig. 6), and the data for HwTx-IV are in agreement with our recently published work (24). Previously published spectra for [E5K,E8K]MfVIA are included as a positive control (45).

Cell culture

Human embryonic kidney 293 (HEK293) cells expressing human $Na_V1.7$ channels along with the β1 auxiliary subunits (SB Drug Discovery, Glasgow, UK) were maintained at 37 °C in a humidified 5% CO_2 incubator in minimum essential medium supplemented with 10% (v/v) heat-inactivated fetal bovine serum, 1% (v/v) GlutaMAX, 0.004 mg/ml blasticidin, and 0.6 mg/ml Geneticin. Cells were subcultured every 3 days in a 1:5 ratio using 0.1% (v/v) trypLE express reagent (Thermo Fisher Scientific) in a T75 flask.

Whole-cell patch-clamp electrophysiology on HEK cells

The inhibitory potency of GMTs on $hNa_V1.7$ stably expressed in HEK293 cells was examined using an automated QPatch-16 electrophysiology platform (Sophion Bioscience, Ballerup, Denmark) at room temperature (~25 °C). The intracellular solution comprised 140 mM CsF, 1 mM EGTA, 5 mM CsOH, 10 mM HEPES, and 10 mM NaCl, pH 7.4, with CsOH (320 mosM). The extracellular solution comprised 2 mM $CaCl_2$, 1 mM $MgCl_2$, 10 mM HEPES, 4 mM KCl, 145 mM NaCl, pH 7.4, with NaOH (305 mosM). Solutions were filtered using a 0.22-μm membrane filter (Merck Millipore, Cork, Ireland). Before recordings, cells were detached from culture flasks with Detachin (Genlantis, San Diego, CA). Na^+ currents were acquired at 25 kHz and filtered at 4 kHz. Cells with <1 nA peak current were excluded. To determine IC_{50} values, $Na_V1.7$ cells were held at −90 mV in the presence of varying concentrations of GMT and then stepped to −120 mV for 200 ms, followed by a 20-ms test depolarization to 0 mV. Na^+ currents were normalized after leak subtraction. Offline analysis was performed using Microsoft Excel and GraphPad Prism version 7. Data are presented as mean ± S.E. of at least three independent experiments.

Two-electrode voltage-clamp electrophysiology

Harvesting of stage V-VI oocytes from ovarian lobes of *Xenopus laevis* and the subsequent expression of $Na_V1.2$, $Na_V1.4$, $Na_V1.5$, and $Na_V1.6$ channels were performed as described (63). After injection with cRNA (50 nl of 1 ng/nl) using a microinjector (Drummond Scientific, Broomall, PA), oocytes were incubated in 96 mM NaCl, 2 mM KCl, 1.8 mM $CaCl_2$, 2 mM $MgCl_2$, and 5 mM HEPES, pH 7.4, supplemented with 50 mg/liter gentamycin sulfate. Whole-cell currents were recorded after 1–4-day incubation periods at room temperature using two-electrode voltage-clamp electrophysiology recordings using a Geneclamp 500 amplifier (Molecular Devices, Downingtown, PA) together with pClamp data acquisition software (Axon Instruments, Union City, CA). The bath solution contained 96 mM NaCl, 2 mM KCl, 1.8 mM $CaCl_2$, 2 mM $MgCl_2$, and 5 mM HEPES, pH 7.4. Voltage and current electrodes were filled with 3 M KCl (resistance 0.8–1.5 megaohms) (63). A four-pole low-pass Bessel filter was used to filter currents at 1 kHz with sampling at 20 kHz. A −P/4 protocol was used for leak subtraction. Currents for Na_V channels were elicited from the oocytes using 30-ms step depolarizations from −90 mV to 70 mV in 5-mV increments. Current traces were obtained by 50-ms depolarizations to V_{max}, the voltage at maximal current in control settings. Modulation of current by GMTs was examined by normalizing the data to peak current amplitude ($I_{30\,ms}/I_{max}$), and concentration–response curves were used to obtain EC_{50} values as before (63). Data are presented as mean ± S.E. of at least three independent experiments. Mature female *X. laevis* were purchased from Nasco (Fort Atkinson, Wisconsin) and were housed in the Aquatic Facility (KU Leuven) in compliance with the regulations of the European Union concerning the welfare of laboratory animals as declared in Directive 2010/63/EU. The use of *X. laevis* was approved by the Animal Ethics Committee of KU Leuven (license number LA1210239, project number P038/2017).

Author contributions—A. J. A., C. I. S., and S. T. H. conceived and designed the study. A. J. A. prepared the manuscript, oxidized the peptides, and conducted NMR, SPR, and fluorescence spectroscopy experiments. A. J. A. and N. L. maintained the HEK cells. S. P. maintained oocytes and conducted two-electrode voltage-clamp electrophysiology. C. Y. C. conducted QPatch experiments. N. L., C. I. S., and S. T. H. assisted A. J. A. with interpretation of data and provided critical reviews of the manuscript. J. T., G. F. K., and D. J. C. provided critical reviews of the manuscript. All authors read the manuscript and provided specific feedback.

Acknowledgments—We thank Olivier Cheneval (Institute for Molecular Bioscience, University of Queensland) for peptide synthesis and Dr. Les Miranda (Amgen) for providing PDB coordinates for GpTx-I.

References

1. Osteen, J. D., Herzig, V., Gilchrist, J., Emrick, J. J., Zhang, C., Wang, X., Castro, J., Garcia-Caraballo, S., Grundy, L., Rychkov, G. Y., Weyer, A. D., Dekan, Z., Undheim, E. A. B., Alewood, P., Stucky, C. L., *et al.* (2016) Selective spider toxins reveal a role for the $Na_V1.1$ channel in mechanical pain. *Nature* **534,** 494–499 CrossRef Medline
2. Kalia, J., Milescu, M., Salvatierra, J., Wagner, J., Klint, J. K., King, G. F., Olivera, B. M., and Bosmans, F. (2015) From foe to friend: using animal toxins to investigate ion channel function. *J. Mol. Biol.* **427,** 158–175 CrossRef Medline
3. Jiang, Y., Lee, A., Chen, J., Ruta, V., Cadene, M., Chait, B. T., and MacKinnon, R. (2003) X-ray structure of a voltage-dependent K^+ channel. *Nature* **423,** 33–41 CrossRef Medline
4. Catterall, W. A., Cestèle, S., Yarov-Yarovoy, V., Yu, F. H., Konoki, K., and Scheuer, T. (2007) Voltage-gated ion channels and gating modifier toxins. *Toxicon* **49,** 124–141 CrossRef Medline

5. Dib-Hajj, S. D., Cummins, T. R., Black, J. A., and Waxman, S. G. (2010) Sodium channels in normal and pathological pain. *Annu. Rev. Neurosci.* **33,** 325–347 CrossRef Medline
6. Lewis, R. J., Vetter, I., Cardoso, F. C., Inserra, M., and King, G. (2015) Does nature do ion channel drug discovery better than us? in *Ion Channel Drug Discovery* (Cox, B., and Gosling, M., eds) pp. 297–319, Royal Society of Chemistry, London, UK
7. Pallaghy, P. K., Nielsen, K. J., Craik, D. J., and Norton, R. S. (1994) A common structural motif incorporating a cystine knot and a triple-stranded β-sheet in toxic and inhibitory polypeptides. *Protein Sci.* **3,** 1833–1839 CrossRef Medline
8. Jung, H. J., Lee, J. Y., Kim, S. H., Eu, Y. J., Shin, S. Y., Milescu, M., Swartz, K. J., and Kim, J. I. (2005) Solution structure and lipid membrane partitioning of VsTx1, an inhibitor of the K_VAP potassium channel. *Biochemistry* **44,** 6015–6023 CrossRef Medline
9. Phillips, L. R., Milescu, M., Li-Smerin, Y., Mindell, J. A., Kim, J. I., and Swartz, K. J. (2005) Voltage-sensor activation with a tarantula toxin as cargo. *Nature* **436,** 857–860 CrossRef Medline
10. Milescu, M., Vobecky, J., Roh, S. H., Kim, S. H., Jung, H. J., Kim, J. I., and Swartz, K. J. (2007) Tarantula toxins interact with voltage sensors within lipid membranes. *J. Gen. Physiol.* **130,** 497–511 CrossRef Medline
11. Smith, J. J., Alphy, S., Seibert, A. L., and Blumenthal, K. M. (2005) Differential phospholipid binding by site 3 and site 4 toxins: implications for structural variability between voltage-sensitive sodium channel domains. *J. Biol. Chem.* **280,** 11127–11133 CrossRef Medline
12. Suchyna, T. M., Tape, S. E., Koeppe, R. E., 2nd, Andersen, O. S., Sachs, F., and Gottlieb, P. A. (2004) Bilayer-dependent inhibition of mechanosensitive channels by neuroactive peptide enantiomers. *Nature* **430,** 235–240 CrossRef Medline
13. Lau, C. H. Y., King, G. F., and Mobli, M. (2016) Molecular basis of the interaction between gating modifier spider toxins and the voltage sensor of voltage-gated ion channels. *Sci. Rep.* **6,** 34333 CrossRef Medline
14. Bosmans, F., and Swartz, K. J. (2010) Targeting sodium channel voltage sensors with spider toxins. *Trends Pharmacol. Sci.* **31,** 175–182 CrossRef Medline
15. Agwa, A. J., Henriques, S. T., and Schroeder, C. I. (2017) Gating modifier toxin interactions with ion channels and lipid bilayers: is the trimolecular complex real? *Neuropharmacology* **127,** 32–45 CrossRef Medline
16. King, G. F., and Vetter, I. (2014) No gain, no pain: $Na_V1.7$ as an analgesic target. *ACS Chem. Neurosci.* **5,** 749–751 CrossRef Medline
17. Salari, A., Vega, B. S., Milescu, L. S., and Milescu, M. (2016) Molecular interactions between tarantula toxins and low-voltage-activated calcium channels. *Sci. Rep.* **6,** 23894 CrossRef Medline
18. Posokhov, Y. O., Gottlieb, P. A., Morales, M. J., Sachs, F., and Ladokhin, A. S. (2007) Is lipid bilayer binding a common property of inhibitor cysteine knot ion-channel blockers? *Biophys. J.* **93,** L20–L22 CrossRef Medline
19. Middleton, R. E., Warren, V. A., Kraus, R. L., Hwang, J. C., Liu, C. J., Dai, G., Brochu, R. M., Kohler, M. G., Gao, Y.-D., Garsky, V. M., Bogusky, M. J., Mehl, J. T., Cohen, C. J., and Smith, M. M. (2002) Two tarantula peptides inhibit activation of multiple sodium channels. *Biochemistry* **41,** 14734–14747 CrossRef Medline
20. Bosmans, F., Rash, L., Zhu, S., Diochot, S., Lazdunski, M., Escoubas, P., and Tytgat, J. (2006) Four novel tarantula toxins as selective modulators of voltage-gated sodium channel subtypes. *Mol. Pharmacol.* **69,** 419–429 Medline
21. Li, D., Xiao, Y., Xu, X., Xiong, X., Lu, S., Liu, Z., Zhu, Q., Wang, M., Gu, X., and Liang, S. (2004) Structure-activity relationships of hainantoxin-IV and structure determination of active and inactive sodium channel blockers. *J. Biol. Chem.* **279,** 37734–37740 CrossRef Medline
22. Xiao, Y., Luo, X., Kuang, F., Deng, M., Wang, M., Zeng, X., and Liang, S. (2008) Synthesis and characterization of huwentoxin-IV, a neurotoxin inhibiting central neuronal sodium channels. *Toxicon* **51,** 230–239 CrossRef Medline
23. Murray, J. K., Ligutti, J., Liu, D., Zou, A., Poppe, L., Li, H., Andrews, K. L., Moyer, B. D., McDonough, S. I., Favreau, P., Stöcklin, R., and Miranda, L. P. (2015) Engineering potent and selective analogues of GpTx-1, a tarantula venom peptide antagonist of the $Na_V1.7$ sodium channel. *J. Med. Chem.* **58,** 2299–2314 CrossRef Medline
24. Agwa, A. J., Lawrence, N., Deplazes, E., Cheneval, O., Chen, R. M., Craik, D. J., Schroeder, C. I., and Henriques, S. T. (2017) Spider peptide toxin HwTx-IV engineered to bind to lipid membranes has an increased inhibitory potency at human voltage-gated sodium channel $hNa_V1.7$. *Biochim. Biophys. Acta* **1859,** 835–844 CrossRef Medline
25. Suchyna, T. M., Johnson, J. H., Hamer, K., Leykam, J. F., Gage, D. A., Clemo, H. F., Baumgarten, C. M., and Sachs, F. (2000) Identification of a peptide toxin from *Grammostola spatulata* spider venom that blocks cation-selective stretch-activated channels. *J. Gen. Physiol.* **115,** 583–598 CrossRef Medline
26. Marvin, L., De, E., Cosette, P., Gagnon, J., Molle, G., and Lange, C. (1999) Isolation, amino acid sequence and functional assays of SgTx-1: the first toxin purified from the venom of the spider *Scodra griseipes*. *Eur. J. Biochem.* **265,** 572–579 CrossRef Medline
27. Wang, J. M., Roh, S. H., Kim, S., Lee, C. W., Kim, J. I., and Swartz, K. J. (2004) Molecular surface of tarantula toxins interacting with voltage sensors in K_V channels. *J. Gen. Physiol.* **123,** 455–467 CrossRef Medline
28. Bosmans, F., Martin-Eauclaire, M.-F., and Swartz, K. J. (2008) Deconstructing voltage sensor function and pharmacology in sodium channels. *Nature* **456,** 202–208 CrossRef Medline
29. Minassian, N. A., Gibbs, A., Shih, A. Y., Liu, Y., Neff, R. A., Sutton, S. W., Mirzadegan, T., Connor, J., Fellows, R., Husovsky, M., Nelson, S., Hunter, M. J., Flinspach, M., and Wickenden, A. D. (2013) Analysis of the structural and molecular basis of voltage-sensitive sodium channel inhibition by the spider toxin huwentoxin-IV (μ-TRTX-Hh2a). *J. Biol. Chem.* **288,** 22707–22720 CrossRef Medline
30. Gui, J., Liu, B., Cao, G., Lipchik, A. M., Perez, M., Dekan, Z., Mobli, M., Daly, N. L., Alewood, P. F., Parker, L. L., King, G. F., Zhou, Y., Jordt, S.-E., and Nitabach, M. N. (2014) A tarantula-venom peptide antagonizes the TRPA1 nociceptor ion channel by binding to the S1–S4 gating domain. *Curr. Biol.* **24,** 473–483 CrossRef Medline
31. Oswald, R. E., Suchyna, T. M., McFeeters, R., Gottlieb, P., and Sachs, F. (2002) Solution structure of peptide toxins that block mechanosensitive ion channels. *J. Biol. Chem.* **277,** 34443–34450 CrossRef Medline
32. Lee, C. W., Kim, S., Roh, S. H., Endoh, H., Kodera, Y., Maeda, T., Kohno, T., Wang, J. M., Swartz, K. J., and Kim, J. I. (2004) Solution structure and functional characterization of SGTx1, a modifier of $K_V2.1$ channel gating. *Biochemistry* **43,** 890–897 CrossRef Medline
33. Agwa, A., Huang, Y.-H., Craik, D., Henriques, S. T., and Schroeder, C. I. (2017) Lengths of the C-terminus and interconnecting loops impact stability of spider-derived gating modifier toxins. *Toxins* **9,** E248 CrossRef Medline
34. van Meer, G., de Kroon, A. I. P. M. (2011) Lipid map of the mammalian cell. *J. Cell Sci.* **124,** 5–8 CrossRef Medline
35. Ramu, Y., Xu, Y., and Lu, Z. (2006) Enzymatic activation of voltage-gated potassium channels. *Nature* **442,** 696–699 CrossRef Medline
36. Milescu, M., Bosmans, F., Lee, S., Alabi, A. A., Kim, J. I., and Swartz, K. J. (2009) Interactions between lipids and voltage sensor paddles detected with tarantula toxins. *Nat. Struct. Mol. Biol.* **16,** 1080–1085 CrossRef Medline
37. Dart, C. (2010) Lipid microdomains and the regulation of ion channel function. *J. Physiol.* **588,** 3169–3178 CrossRef Medline
38. Henriques, S. T., Deplazes, E., Lawrence, N., Cheneval, O., Chaousis, S., Inserra, M., Thongyoo, P., King, G. F., Mark, A. E., Vetter, I., Craik, D. J., and Schroeder, C. I. (2016) Interaction of tarantula venom peptide ProTx-II with lipid membranes is a prerequisite for its inhibition of human voltage-gated sodium channel $Na_V1.7$. *J. Biol. Chem.* **291,** 17049–17065 CrossRef Medline
39. Deplazes, E., Henriques, S. T., Smith, J. J., King, G. F., Craik, D. J., Mark, A. E., and Schroeder, C. I. (2016) Membrane-binding properties of gating modifier and pore-blocking toxins: membrane interaction is not a prerequisite for modification of channel gating. *Biochim. Biophys. Acta* **1858,** 872–882 CrossRef Medline
40. Hunte, C., and Richers, S. (2008) Lipids and membrane protein structures. *Curr. Opin. Struct. Biol.* **18,** 406–411 CrossRef Medline

41. Palsdottir, H., and Hunte, C. (2004) Lipids in membrane protein structures. *Biochim. Biophys. Acta* **1666,** 2–18 CrossRef Medline
42. Henriques, S. T., Huang, Y. H., Castanho, M. A., Bagatolli, L. A., Sonza, S., Tachedjian, G., Daly, N. L., and Craik, D. J. (2012) Phosphatidylethanolamine binding is a conserved feature of cyclotide-membrane interactions. *J. Biol. Chem.* **287,** 33629–33643 CrossRef Medline
43. Lakowicz, J. R. (2006) *Principles of Fluorescence Spectroscopy*, 3rd Ed., pp. 277–330, Springer Science+Business Media, New York, NY
44. Ladokhin, A. S., Jayasinghe, S., and White, S. H. (2000) How to measure and analyze tryptophan fluorescence in membranes properly, and why bother? *Anal. Biochem.* **285,** 235–245 CrossRef Medline
45. Deuis, J. R., Dekan, Z., Inserra, M. C., Lee, T. H., Aguilar, M. I., Craik, D. J., Lewis, R. J., Alewood, P. F., Mobli, M., Schroeder, C. I., Henriques, S. T., and Vetter, I. (2016) Development of a muO-conotoxin analogue with improved lipid membrane interactions and potency for the analgesic sodium channel $Na_V1.8$. *J. Biol. Chem.* **291,** 11829–11842 CrossRef Medline
46. Xiao, Y., Bingham, J. P., Zhu, W., Moczydlowski, E., Liang, S., and Cummins, T. R. (2008) Tarantula huwentoxin-IV inhibits neuronal sodium channels by binding to receptor site 4 and trapping the domain II voltage sensor in the closed configuration. *J. Biol. Chem.* **283,** 27300–27313 CrossRef Medline
47. Takahashi, H., Kim, J. I., Min, H. J., Sato, K., Swartz, K. J., and Shimada, I. (2000) Solution structure of hanatoxin1, a gating modifier of voltage-dependent K^+ channels: common surface features of gating modifier toxins. *J. Mol. Biol.* **297,** 771–780 CrossRef Medline
48. Jung, H. H., Jung, H. J., Milescu, M., Lee, C. W., Lee, S., Lee, J. Y., Eu, Y.-J., Kim, H. H., Swartz, K. J., and Kim, J. I. (2010) Structure and orientation of a voltage-sensor toxin in lipid membranes. *Biophys. J.* **99,** 638–646 CrossRef Medline
49. Lee, S.-Y., and MacKinnon, R. (2004) A membrane-access mechanism of ion channel inhibition by voltage sensor toxins from spider venom. *Nature* **430,** 232–235 CrossRef Medline
50. Schmalhofer, W. A., Calhoun, J., Burrows, R., Bailey, T., Kohler, M. G., Weinglass, A. B., Kaczorowski, G. J., Garcia, M. L., Koltzenburg, M., and Priest, B. T. (2008) ProTx-II, a selective inhibitor of $Na_V1.7$ sodium channels, blocks action potential propagation in nociceptors. *Mol. Pharmacol.* **74,** 1476–1484 CrossRef Medline
51. Swartz, K. J., and MacKinnon, R. (1997) Mapping the receptor site for hanatoxin, a gating modifier of voltage-dependent K^+ channels. *Neuron* **18,** 675–682 CrossRef Medline
52. Cai, T., Luo, J., Meng, E., Ding, J., Liang, S., Wang, S., and Liu, Z. (2015) Mapping the interaction site for the tarantula toxin hainantoxin-IV (β-TRTX-Hn2a) in the voltage sensor module of domain II of voltage-gated sodium channels. *Peptides* **68,** 148–156 CrossRef Medline
53. Liu, Y., Li, D., Wu, Z., Li, J., Nie, D., Xiang, Y., and Liu, Z. (2012) A positively charged surface patch is important for hainantoxin-IV binding to voltage-gated sodium channels. *J. Pept. Sci.* **18,** 643–649 CrossRef Medline
54. King, G. F., and Hardy, M. C. (2013) Spider-venom peptides: structure, pharmacology, and potential for control of insect pests. *Annu. Rev. Entomol.* **58,** 475–496 CrossRef Medline
55. Gao, Y., Cao, E., Julius, D., and Cheng, Y. (2016) TRPV1 structures in nanodiscs reveal mechanisms of ligand and lipid action. *Nature* **534,** 347–351 CrossRef Medline
56. Ostrow, K. L., Mammoser, A., Suchyna, T., Sachs, F., Oswald, R., Kubo, S., Chino, N., and Gottlieb, P. A. (2003) cDNA sequence and *in vitro* folding of GsMTx4, a specific peptide inhibitor of mechanosensitive channels. *Toxicon* **42,** 263–274 CrossRef Medline
57. Wüthrich, K. (1986) *NMR of Proteins and Nucleic Acids*, Wiley Interscience, New York
58. Fraczkiewicz, R., and Braun, W. (1998) Exact and efficient analytical calculation of the accessible surface areas and their gradients for macromolecules. *J. Comput. Chem.* **19,** 319–333 CrossRef
59. Baker, N. A., Sept, D., Joseph, S., Holst, M. J., and McCammon, J. A. (2001) Electrostatics of nanosystems: application to microtubules and the ribosome. *Proc. Natl. Acad. Sci. U.S.A.* **98,** 10037–10041 CrossRef Medline
60. Gill, S. C., and von Hippel, P. H. (1989) Calculation of protein extinction coefficients from amino acid sequence data. *Anal. Biochem.* **182,** 319–326 CrossRef Medline
61. Henriques, S. T., Huang, Y. H., Rosengren, K. J., Franquelim, H. G., Carvalho, F. A., Johnson, A., Sonza, S., Tachedjian, G., Castanho, M. A., Daly, N. L., and Craik, D. J. (2011) Decoding the membrane activity of the cyclotide kalata B1: the importance of phosphatidylethanolamine phospholipids and lipid organization on hemolytic and anti-HIV activities. *J. Biol. Chem.* **286,** 24231–24241 CrossRef Medline
62. Henriques, S. T., Pattenden, L. K., Aguilar, M.-I., Castanho, M. A. R. B. (2009) The toxicity of prion protein fragment PrP(106–126) is not mediated by membrane permeabilization as shown by a M112W substitution. *Biochemistry* **48,** 4198–4208 CrossRef Medline
63. Peigneur, S., Cologna, C. T., Cremonez, C. M., Mille, B. G., Pucca, M. B., Cuypers, E., Arantes, E. C., and Tytgat, J. (2015) A gamut of undiscovered electrophysiological effects produced by *Tityus serrulatus* toxin 1 on Na_V-type isoforms. *Neuropharmacology* **95,** 269–277 CrossRef Medline